ELSEVIER

Journal of Nuclear Materials 302 (2002) 109–124

journal of nuclear materials

www.elsevier.com/locate/jnucmat

# On the nuclear oxide fuel densification, swelling and thermal re-sintering

M.C. Paraschiv [a,*], A. Paraschiv [a], V.V. Grecu [b]

[a] *Institute for Nuclear Research, P.O. Box 78, R-0300 Pitesti, Romania*
[b] *Faculty of Physics, University of Bucharest, P.O. Box MG-11 Bucharest, Romania*

Received 1 October 2001; accepted 6 February 2002

**Abstract**

A method of calculating the fuel densification and swelling as a result of only the initial fuel porosity has been developed. Well-characterized $UO_2$ fuel pellets, from the Romanian CANDU type fuel fabrication route, were used to fit the specific pore volume distribution resulted from the sintering process to a lognormal distribution function and thermal re-sintering tests up to 280 h at 1700 °C were done to fit the coefficients of vacancies diffusion and the self-diffusion of uranium, required by the model. Careful analyses proved that the irradiation-induced resolution is strongly dependent of the hydrostatic pressure and a corrected formula has been proposed. Analyses of the time evolution of the pore size distribution during re-sintering tests and annealing tests similar with some as described in the open literature were also done. © 2002 Elsevier Science B.V. All rights reserved.

## 1. Introduction

Sintering from compacted $UO_2$ powders at high temperature (1600–1700 °C) in controlled atmosphere, during the fabrication route results in high density fuel pellets including a pore size distribution whose characteristics controls the rate of volume change at the beginning of irradiation. The resulting fuel pellets have a small amount of porosity remained after the fuel sintering. The porosity, consisting of small pores of various sizes, becomes important during the fuel irradiation because, by pores shrinkage as a result of operating temperature of the nuclear fuel, the dimensional stability of the pellets will be affected.

The fission gas atoms resulted from the fission process are accumulated in the as-fabricated pores but also in the vacancy clusters left in the wake of the fission fragments and new gas bubbles are generated inside the fuel. All these processes involve dimensional changes and failure of the physical parameters of the fuel. Many attempts to give a satisfactory description of the time evolution of the remaining porosity and of gas bubbles nucleating and growth were done but the particular characteristic of volume changing of the oxide fuel during the irradiation has been treated using two distinct manners.

One of them refers to the fuel densification, which is an important feature of the fuel pellets affecting their dimensional stability, and whose kinetics is governed by the as-fabricated pore size distribution. Thermal re-sintering tests on fuel pellets from the fabrication route were currently done to simulate in-reactor fuel densification.

The other one refers to the gas swelling of the fuel matrix. Often, the theoretical results were used as support of specific post irradiation annealing tests.

But, intra- and inter-granular bubbles swelling and the reducing of the pore sizes from the as-fabricated porosity will compete to the time evolution of the fuel pellets volume. Both the operating temperature and the irradiation conditions controls the two as-described processes denoted as the gas swelling and the fuel densification.

* Corresponding author. Tel.: +40-48 213 400x389; fax: +40-48 262 449.
*E-mail address:* mariusparaschiv@mail.rtns.ro (M.C. Paraschiv).

0022-3115/02/$ - see front matter © 2002 Elsevier Science B.V. All rights reserved.
PII: S0022-3115(02)00797-3

Historically, the fuel densification was associated to the fuel elements behavior during the first in reactor-irradiation days. That is, only those characteristics of the fuel pellet such as the fraction of the fine pores that is directly correlated to the initial rate of the fuel densification was careful analyzed.

It is generally accepted that the amount of the fine pores of radius $R_p < 0.05$ μm has a great effect on the kinetics of the volume changes of the fuel pellets both during the re-sintering tests and during the fuel irradiation [1,2,5]. Moreover, even for the same type of the fuel elements, the technological process of fuel fabrication (especially the flowing properties of the $UO_2$ powder and consequently the sintering parameters) will affect the pore size distribution and the kinetics of fuel densification will be implicitly different. Such situation has been observed to the experimental tests on the Romanian CANDU type fuel in both NRU-AECL and TRIGA-INR reactors where the measured fuel deformations were greater than predicted using the empirical densification laws established on Canadian experiments from published information [9,10,12–14].

Often, empirical densification laws were proposed to avoid the modelling difficulties [10,11,15] that can be used only for particular situations.

It is known [16] that the irradiation-induced point defects accelerate the fuel densification. Most of the point defects created by a fission fragment collapse into damage cascades in its wake but ~10% are allowed to escape. The interstitials migrate to the various trapping sites, such as the dislocations or the grain boundaries or can be loosed by mutual recombination, faster than vacancies move into the fuel lattice, so that the vacancies migration will control the real balance of the volume change of the fuel pellets. The fission spikes interact with the pores and an excess of vacancies concentration will appear surrounding the pore. Speight [19] shown that, whereas absorption of interstitials can lead to void shrinkage, the free vacancies cannot reach grain boundaries so fast at the fuel elements operating temperatures and hence the overall pellet density can only increase to a very limited extent by lattice relaxation.

Because the fuel densification and the gaseous fuel swelling are generally treated as separate processes, the importance of the dislocations on the vacancies balances in oxide fuel has been pointed out rather in that works dedicated to the modelling of the intra-granular bubbles swelling [20,34,35,43] than the fuel densification. A description of the fuel densification considering the migration of point defects (both the interstitials and the vacancies) to pores and dislocations resulted from the Dollins and Nichols model [3,5], which unfortunately neglected the effect of the initial pore size distribution on the kinetics of fuel densification. Bouguera and Si-Ahmed [7] completed their model to consider an arbitrary pore size distribution. Detailed experimental results regarding the irradiation and temperature dependence of the pore size distribution were given in Ref. [6]

High-pressure argon atmosphere was used to simulate the inter-granular bubbles swelling [39] and thermal re-sintering on $UO_2$ fuel pellets [8]. Kashibe and Une proved a very simple correlation previously established by Hull and Rimmer [40]. The correlation is derived from the creep tests in metals and it is however unproper used because it not consider the complex processes involved in oxide fuel densification and swelling during the fuel irradiation.

The intra-granular bubbles nucleation and growing were the subject of an extensive work both experimental and theoretical. Wapham [24] suggested that a sputtering mechanism is responsible of the observed re-solution rates of gas atoms in uranium dioxide and Cornell and Turnbull shown by direct measurements and calculation the existence of a critical dose at which the bubble population is stable and proved that the effect of the irradiation-induced resolution is to prevent established bubbles to collect fission gas trough-out the whole irradiation time [23,26,27]. Turnbull [25] gave a value of the irradiation-induced resolution parameter and, based on experimental data, he established a bubble growth law and a bubble size distribution of the form $C_B(R)R^2 =$ const., where $C_B(R)$ is the concentration of the bubbles of the radius $R$. His simple model has been fitted with good result on some experimental data. Based on his model Turnbull concluded that the amount of gas contained in the intra-granular bubbles is negligible small and their contribution to the gas release models must be ignored.

It is worth mentioning the Speight's model [28] regarding the relationship of the intra-granular concentration of fission gas existing instantaneously within the bubbles and in solution, extended to account for the inter-granular bubble resolution. The inter-granular model has been extended to simultaneously evaluate the fission gas release using a grain size distribution function [29].

Other mechanisms by which the intra-granular bubbles nucleate and grow, such as random bubble migration and coalescence [31] or accumulation by random migration at the dislocations [20], bubble coalescence and migration in thermal gradient, have been proposed and complex models and computation codes to evaluate the fission gas evolution in oxide fuels during irradiation have been developed [21,31–35].

The stress field resulted from the pellet-cladding mechanical contact, also affects the temperature and fission gas induced pellet-volume changes [41]. The effect of the stress field on the volume changes considering both the gas swelling and the as-fabricated porosity acting as fission gas sinks has been studied by Blank [30], but only in the simple case of in-equilibrium bubbles and pores. He also calculated a critical radius of the bubble from which the bubble growth becomes unstable.

Notley and Hastings in their model [32] used the balance of fission gas diffusion in both as-fabricated porosity and a fixed number of inter-granular bubbles in equilibrium at the grain boundary.

To evaluate the intra-granular bubbles behavior during fast annealing tests at 150 K/s of the irradiated fuel, a model of thermal resolution of fission gas atoms from bubbles together with single atom diffusion to grain boundaries has been proposed in Ref. [36,37].

Evans [44] pointed out that experimental results and the calculated solution energies of fission gases in Ref. [45] disregard with the assumption of their thermal resolution in gas bubbles. Based on the experimental evidence that intra-granular bubbles have larger sizes near the grain boundary than inside the grain, Evans advanced a new model in which the inherent vacancy gradient from the grain boundary to its center allows the bubbles not only to grow but also to migrate to the grain boundary [44].

An alternative model suggests that the elastic field around the bubbles increases with gas precipitation and does finally lead to lowering of the precipitation rate [38] in conditions of a rapid diffusion rate comparatively with the microscopic plastic deformation rate. In heterogeneous media this effect improves gas precipitation in places where vacancy availability is higher. Consequently, a large amount of gas precipitates on grain boundaries and dislocations. We suppose that the theory is particularly good when isolated bubbles are studied. In a global analysis, we have to assume a homogeneous distribution of the dislocations and rather new gas bubbles arise near the dislocations than improving of the fission gas migration to that places where the vacancy availability is higher. Of course, the amount of the fission gas released inside the void volume of the fuel elements will be retarded by its accumulation in the matrix voids of the fuel and, correlated to this, the remaining porosity could accumulate an excess of gas concentration to be considered in such analyses. So, the fission gas release and the initial distribution of the pore sizes would be correlated and cannot be separately described. Besides the fission gas diffusion to the grain boundary, an accurate description of the oxide fuel behavior during irradiation requires an adequate treatment of the intragranular bubble swelling, especially during the temperature transients. Experimental results shown that a bimodal distribution of intra-granular bubbles raises during the annealing tests on irradiated fuel [42]. The size distribution of the larger bubbles is of the form of an exponential tail and their concentration is about five orders of magnitude lower than the initial bubble concentration and so, close to the initial as-fabricated porosity.

The purpose of the paper is to set up the possibility to evaluate the fuel densification and swelling as a result of the initial fuel porosity using a method, which considers the grain boundaries, the fission fragments interaction with the fuel matrix and pores and also the linear defects as sources and sinks of vacancies. The weights of some parameters such as dislocation density, pore concentrations and grain growth effect on fuel re-sintering, densification and swelling are also evaluated. Thermal re-sintering tests used to evaluate the model parameters are described. Some analyses regarding the availability of the former pore regions to eventually contribute at the new large bubble population, which develop during the post irradiation annealing tests, will be done.

The intra- and inter-granular bubble nucleation and swelling are not treated however. Only those characteristics that are similar with the initial pores evolution during the oxide fuel irradiation are analyzed.

## 2. Fuel characterization and experimental results

As an application of the theoretical results presented below, some characteristics of the fuel pellets from the fabrication route of the Romanian CANDU type fuel elements will be described in the follows. The experimental results from thermal re-sintering tests made on the Romanian $UO_2$ fuel will be used to fit the physical parameters (the self-diffusion coefficient of the $U^{4+}$ cations and the thermal diffusion coefficient of vacancies) requested by the model.

To see how different the pore size distribution of the Romanian manufactured fuel pellets versus the Canadian manufactured fuel pellets is, and to verify the stability of the technological fabrication process, an initial number of 19 archive fuel pellets representing 12 fuel batches manufactured between 1987–1988 years have been selected [15]. The pellets densities were measured using the xylene immersion penetration method [15] and analyzed for pore size distribution using an automatic image analyses system including a LEITZ optical microscope from the INR hot cell laboratory [17]. About 1500–2000 pores have been detected and measured for every sample. Their sizes have been grouped in 8–9 of equal length size classes between 0.42–8 μm.

The pore volumes from every size class have been evaluated and the pore volume frequency histogram obtained was fitted to a lognormal distribution function using the Levenberg–Marquardt algorithm. Such evaluations were made for each fuel pellet analyzed and the results are given in Table 1. Not all the archive pellets could be fitted to a lognormal distribution function, very few of them having a radial distribution of the pore size. They were eliminated from the analyses of pore distribution. The other measured fuel pellets had very closed values of the distribution parameters and it has been concluded that they could be samples of a unique pore size distribution representing the manufacturing technology. As it can be seen in Table 1, the estimated

Table 1
The estimated average diameter, standard deviation and the corresponding parameters of the lognormal distribution functions resulted by fitting the pore size measurements ([Ref. [15]])

| Lot | 883 | 155-OA | 172-OP | 187 | 224 | 242 | 249 | 288 | 740 |
|---|---|---|---|---|---|---|---|---|---|
| size (μm) | 1.61 | 1.82 | 1.92 | 2.44 | 1.95 | 1.92 | 2.43 | 2.55 | 1.59 |
| $\sigma$ | 0.8741 | 1.1292 | 1.0540 | 1.8172 | 1.1989 | 1.0782 | 2.24 | 2.3720 | 0.8067 |
| $m$ | 0.34495 | 0.43907 | 0.52308 | 0.66896 | 0.50672 | 0.51602 | 0.58018 | 0.62278 | 0.34014 |
| $s$ | 0.50904 | 0.56951 | 0.51235 | 0.66523 | 0.56654 | 0.52327 | 0.78453 | 0.79020 | 0.48186 |

average diameter (1.6–2.5 μm) and standard deviation (0.8–2.4 μm) are very close each other.

The densities resulted by pore numbering, by integration of the resulted lognormal distribution functions and by immersion technique are given in Table 2. It can be seen in Table 2 that closer values versus the immersion technique of the fuel densities resulted by integration of the fitted lognormal distribution function rather than from the pore numbering. The difference can be explained if we take into account that the pores whose radius was smaller that 0.42 μm could not be detected but can be estimated using the corresponding integration area from the lognormal distribution function.

The hypothesis regarding the lognormal characteristic of the pore size distribution has been confirmed both by comparisons with the immersion results and by fitting coefficients. The homogeneity Cochran test of the variances of $K$ normal populations and $\Lambda$-Neyman–Pearson tests of general homogeneity of both average values and variances were applied to the results depicted in Table 2. Both of them confirmed for 5% confidence level that the measured pore sizes distributions are samples from a unique lognormal population of the following parameters:

$$\widehat{\mu} = \frac{1}{k}\sum_{i=1}^{k}\mu_i = 0.5046; \quad \widehat{s} = \sqrt{\frac{1}{k}\sum_{i=1}^{k}s_i^2} = 0.6105.$$

It follows that the estimated average pore diameter of the Romanian CANDU type fuel is $\Phi_{\mathrm{INR}} = 2.00$ μm, and the standard deviation $\sigma_{\mathrm{INR}} = 1.34$ μm, which are greater versus the Canadian CANDU type fuel whose values are $\Phi_{\mathrm{AECL}} = 0.50$ μm, respectively $\sigma_{\mathrm{AECL}} = 0.58$ μm [9]. The resulted pore size distribution of the Romanian CANDU type fuel is given in Fig. 2(a). So, the greater measured fuel elements deformations of the Romanian CANDU type fuel versus the similar Canadian CANDU type fuel during the irradiation tests are the result of the different pore size distribution of the two manufacturers.

Current fuel characterisation works use SEM to supplement optical microscopy in the study of porosity size distribution. The results reveal a large population of

Table 2
The densities resulted by pore numbering, by integration of the resulted lognormal distribution functions and by xylene immersion technique on $UO_2$ pellets from the Romanian fabrication route used to evaluate the pore size distribution (Ref. [15])

| Sample | Fuel density (g/cm$^3$) | | | Porosity (%) | | |
|---|---|---|---|---|---|---|
| | Xylene immersion | Pore numbering | Fitting to a lognormal | Xylene immersion | Pore numbering | Fitting to a lognormal |
| 083/2 | 10.67 | 10.65 | 10.65 | 2.637 | 2.837 | 2.826 |
| 155/OA/1 | 10.57 | 10.50 | 10.47 | 3.522 | 4.175 | 4.499 |
| 172/OP/1 | 10.49 | 10.48 | 10.46 | 4.279 | 4.348 | 4.554 |
| 187/1 | 10.54 | 10.64 | 10.59 | 3.796 | 2.884 | 3.396 |
| 224-2 | 10.52 | 10.56 | 10.53 | 4.005 | 3.608 | 3.888 |
| 242-1 | 10.58 | 10.61 | 10.57 | 3.504 | 3.186 | 3.355 |
| 740-1 | 10.63 | 10.63 | 10.63 | 3.047 | 2.971 | 3.001 |
| 249-6 | 10.64 | 10.74 | 10.68 | 2.920 | 2.052 | 2.563 |
| 249-1 | 10.63 | 10.63 | 10.57 | 2.993 | 2.979 | 3.550 |
| 288-1 | 10.58 | 10.61 | 10.54 | 3.513 | 3.212 | 3.902 |
| 288-3 | 10.63 | 10.69 | 10.66 | 2.984 | 2.445 | 2.762 |
| 288-7 | 10.60 | 10.63 | 10.59 | 3.248 | 2.994 | 3.400 |
| 288-9 | 10.72 | 10.75 | – | 2.190 | 1.907 | – |
| 271-5 | 10.71 | 10.78 | – | 2.281 | 1.756 | – |

Table 3
The densities of the fuel pellets from the batches no. 249, 271 and 288, during the thermal re-sintering tests at 1700 °C, resulted from xylene immersion method

| Sample | Time (h) | | | | | | | |
|---|---|---|---|---|---|---|---|---|
| | 0 | 5 | 15 | 30 | 60 | 100 | 172 | 280 |
| 249-P1 | 10.642 | 10.632 | – | – | – | – | – | – |
| 249-P2 | 10.677 | 10.667 | 10.666 | 10.666 | 10.676 | 10.679 | 10.671 | 10.679 |
| 249-P3 | 10.657 | 10.652 | 10.653 | 10.657 | 10.660 | 10.663 | 10.657 | 10.660 |
| 271-P1 | 10.605 | – | – | – | – | – | – | – |
| 271-P2 | 10.613 | 10.625 | 10.644 | – | – | – | – | – |
| 271-P3 | 10.606 | 10.625 | 10.643 | 10.664 | – | – | – | – |
| 271-P4 | 10.594 | 10.610 | 10.624 | 10.649 | 10.674 | 10.689 | 10.695 | 10.713 |
| 271-P5 | 10.599 | 10.616 | 10.633 | 10.652 | 10.678 | 10.694 | 10.695 | 10.710 |
| 288-P1 | 10.575 | – | – | – | – | – | – | – |
| 288-P2 | 10.595 | 10.608 | 10.624 | 10.649 | 10.675 | 10.690 | 10.702 | 10.720 |
| 288-P3 | 10.578 | 10.589 | 10.604 | – | – | – | – | – |
| 288-P4 | 10.606 | 10.617 | 10.631 | 10.657 | 10.676 | 10.691 | 10.706 | 10.720 |
| 288-P5 | 10.573 | 10.586 | 10.601 | 10.622 | 10.644 | 10.656 | 10.665 | 10.681 |
| 288-P6 | 10.583 | 10.594 | 10.612 | 10.634 | 10.652 | 10.670 | 10.680 | 10.694 |
| 288-P7 | 10.581 | 10.594 | 10.610 | 10.633 | – | – | – | – |
| 288-P8 | 10.560 | 10.575 | 10.590 | 10.609 | 10.636 | 10.652 | 10.659 | 10.681 |
| 288-P9 | 10.592 | 10.610 | 10.629 | 10.651 | 10.674 | 10.693 | 10.704 | 10.720 |

sub-micron diameter pores, previously unresolvable, which can contribute up to 30% of the total pore volume [49]. The volume fraction of the pores with sizes smaller than the smallest limit resulted from our analyses by optical microscopy is $\mathrm{Erf}[\mathrm{Ln}(0.42), \mu, s] \approx 0.23$ (Erf is the error function) or 23% from the total. Without any underestimation of the importance of the SEM analyses in fuel characterization, the fitting methods used to complete the leakage of information about the pores size distribution beyond the lowest limit resulted by optical microscopy proves the powerful of the statistical tools in such kind of analyses.

To arrive at a densification law specific for the Romanian CANDU type fuel, re-sintering tests at 1700 °C on fuel pellets extracted from five batches from the fabrication route were done. The fuel pellets densities were measured by xylene immersion technique after 5, 15, 30, 60, 100, 172 and 280 h. Pore size distributions have been measured after 15, 30 h and respectively at the end of the re-sintering tests (280 h) [15,17]. The measured values of the densities of the fuel pellets batch no. 288 are given in Table 3 and the corresponding pore size distribution resulted by fitting to a lognormal function (whose parameters can be taken from Table 2) is shown in Fig. 2(b). As it can be seen in Table 3 the final densities of the fuel pellets can be correlated with their initial densities. Thus the fuel pellet that had an initial greater density will have all the time of the re-sintering test a greater density. The differences become smaller at the end of the re-sintering test, which means that the fuel densification could cease after 280 h of thermal treatment at 1700 °C.

## 3. Theoretical treatment

To give a solution to the problem of the fuel densification and swelling, most of the models begin with the definition of the thermal flux at the surface of an arbitrary pore of radius $R_p$ derived from the solution of the steady state diffusion equation of point defects associated to a void embedded into an infinite medium. In such cases, the thermal rate of vacancy diffusion at the pore surface is

$$Q_{\mathrm{th}} = 4\pi R_p D_v^{\mathrm{th}} \left( C_v^{\mathrm{eq}} e^{p\Omega/k_B T} - C_v \right), \tag{1}$$

where, $D_v^{\mathrm{th}}$ is the thermal diffusion coefficient of vacancies, $\Omega$ is the atomic volume, $C_v^{\mathrm{eq}}$ is the thermal equilibrium concentration of the vacancies, $p$ is the pressure in excess at the void's surface,

$$p = \frac{2\gamma}{R_p} + p_h - p_g, \tag{2}$$

$\gamma$ is the surface tension, $p_h$ is the hydrostatic pressure, $p_g$ is the gas pressure inside the void volume and $C_v$ is the vacancies concentration at an infinite distance from the void.

The mechanisms for thermal sintering involving Eq. (1) remain valid in-pile but the kinetics are significantly modified through an effective diffusion coefficient [1,2,4],

$$D_v = D_0^{irr}\dot{F} + D_0^{th}\exp\left(-\frac{Q_{th}}{RT}\right), \tag{3}$$

where $\dot{F}$ is the fission rate, $Q_{th}$ is the thermal activation energy of diffusion and $D_0^{irr}$, $D_0^{th}$ must be fitted empirically [5].

Assmann and Stehle defined the fission spike interaction with the pores as being proportionally with the pore surface for coarse pores as follows:

$$Q_{irr} = 2\pi R_p^2 \dot{F}\mu N_v \Omega\left(1-\frac{C_v}{C_s}\right), \tag{4}$$

where $\mu$ is the average track length of a fission fragment, and the saturation concentration $C_s$ was used to give a better fit of the model to their results [2].

Generation of vacancies by fission spikes in the lattice [3] and the vacancies absorption to the linear defects must be included by a term,

$$q_f = \beta n_v \Omega\dot{F} - Z_v\rho_d D_v\left(C_v - C_v^{eq}\right), \tag{5}$$

where $n_v$ is the number of vacancies from a fission event, $\beta$ is the fraction that do not immediately recombine, $Z_v/a$ is the number of sink sites of vacancies per unit length of dislocation ($a$ is lattice parameter), $\rho_d$ is the density of the linear dislocations (in units of length per unit volume).

The solutions given to Eqs. (1) and (4) require the knowledge of the local vacancies concentration $C_v$ [1–3]. In our analyses we will replace the local vacancies concentration with the vacancies concentration averaged everywhere in the system using an homogenized source term of the form [4]

$$q = \int_0^\infty (Q_{th} + Q_{irr})N(R_p)\,dR_p + q_f \tag{6}$$

to solve the diffusion equation associated to the vacancies migration inside of an arbitrary grain under quasi-equilibrium conditions. The expression of the diffusion equation for an arbitrary size grain, with the source term defined by Eq. (6) is

$$\frac{1}{r^2}\frac{d}{dr}\left(r^2\frac{dC_v'}{dr}\right) + \frac{q}{D_v} = 0; \quad \left.\frac{dC_v'}{dr}\right|_{r=0} = 0;$$
$$C_v'(r_g) = C_{gb} = C_v^{eq}\exp\left(\frac{p_h\Omega}{k_B T}\right). \tag{7}$$

To account for the arbitrary void position inside the pellets volume, the solution of Eq. (7) will be averaged using the grain volume distribution function $g(V_g)$, which is characteristic to the polycrystalline material,

$$C_v = 4\pi\int_0^\infty g(V_g)\int_0^{r_g} C_v'(r')r'^2\,dr'\,dV_g. \tag{8}$$

Now, using the notations

$$a^2 = 4\pi C_B\left[\frac{D_v^{th}}{D_v}\overline{R}_p + \frac{F\mu N_v\Omega}{2D_v C_s}\overline{R_p^2}\right] + Z_v\rho_d,$$

$$b = 4\pi C_B\left[\frac{D_U}{D_v}\int_0^\infty R_p e^{\frac{p\Omega}{k_B T}} n(R_p)\,dR_p + \frac{F\mu N_v\Omega}{2D_v}\overline{R_p^2}\right] + \frac{n_v\beta\Omega F}{D_v} + Z_v\rho_d C_v^{eq}, \tag{9}$$

$$\overline{R}_p = \int_0^\infty R_p n(R_p)\,dR_p; \quad \overline{R_p^2} = \int_0^\infty R_p^2 n(R_p)\,dR_p,$$

where $D_U = C_v^{eq}D_v^{th}$, and $n(R_p) = N(R_p)/C_B$; $C_B$ the pore concentration in the unit volume, then solving Eq. (7) and substituting the solution in Eq. (8), after arrangement of terms it will result in

$$C_v = \frac{C_{gb} + bA}{1 + a^2 A}; \quad A = \frac{4\pi}{45}\int_0^\infty r_g^5 g(V_g)\,dV_g. \tag{10}$$

In Eq. (10) we assumed that $\int_0^\infty V_g g(V_g)\,dV_g = 1$.

From the vacancies balance at the surface of an arbitrary pore,

$$\frac{dV_p}{dt} = -\Omega J_p = -Q_{th} - Q_{irr}, \tag{11}$$

whose form in terms of pore radius $R_p$ is

$$\frac{dR_p}{dt} = -\frac{D_v^{th}}{R_p}\left(C_v^{eq}e^{\frac{p\Omega}{k_B T}} - C_v\right) - \frac{\dot{F}\mu N_v\Omega}{2C_s}(C_s - C_v). \tag{12}$$

From definition (Eq. (10)) the average vacancies concentration from the matrix is associated to the grains size by only the $A$ parameter. Or, in other words the fuel densification is dependent on the grain volume distribution function only in the case of grain growth. Otherwise, even in absence of the irradiation, for a constant value of the $A$ parameter the fuel will still shrink, which is different versus the Coble model where the fuel densification take place only if the grains grow in time [2,46].

The rate of gas density change into the pore $n_g$ is

$$\frac{dn_g}{dt} = 4\pi D_g C_g R_p - b_0 n_g, \tag{13}$$

where $D_g$ is the diffusion coefficient of the fission gases inside the fuel matrix, $C_g$ is the average gas concentration from the matrix and $b_0$ the rate of irradiation-induced resolution. From Ref. [16],

$$b_0 = 1.7\times 10^{-17}\eta F\ (s^{-1});$$
$$\eta = 1 - \left\{1 - 15\left[\frac{1}{R_p} + \frac{1}{B}\left(\frac{k_B T}{2\gamma}\right)\right]\right\}^3;$$
$$B = 85\ \text{Å}^3.$$

It has been often supposed that the fission gas migrated in pore obeys the van der Waals equation,

$$p_g\left(\frac{1}{n_g}-b\right)=kT,$$

where $b$ is the van der Waals constant. The van der Waals equation becomes unpractical in analyses regarding the gas accumulated in intra-granular bubbles, because their gas concentration is usually closed to the $b$ constant and mathematically the gas pressure tends to infinite. Harisson recommended the using of an extrapolated equation of state in which gas pressure values as function of the gas density and temperature are tabulated [22]. He also found that the Xe density in liquid phase is higher than predicted using the van der Waals constant. His interpolation table was used in to evaluate the fission gas pressures from intra-granular bubbles in the follows.

Because of the mechanical contact between the fuel and cladding, the effect of the hydrostatic pressure on the resolution efficiency $\eta$ introduced by Nelson [16] cannot be neglected and from Eq. (14) its form in such cases becomes

$$\eta=1-\left\{1-15\left[\frac{1}{R_p}+\frac{1}{B}\left(\frac{k_BT}{2\gamma+p_HR_p}\right)\right]\right\}^3;$$
$$\lim_{p_H\to\infty}\eta=1-\left(1-\frac{15}{R_p}\right)^3. \tag{15}$$

As can be seen in Fig. 1 even at lower hydrostatic pressures the resolution efficiency could change with an order of magnitude. For greater values of the hydrostatic pressure the resolution efficiency goes down to the horizontal asymptote given in Eq. (15), that means that very slow amount of fission gas would be extracted from the pore by interaction with the fission fragments [16]. At lower pore radius (~15 Å) the resolution efficiency $\eta=1$.

Generally, the hydrogen is used as sintering atmosphere. An initial hydrogen atoms concentration can be evaluated from

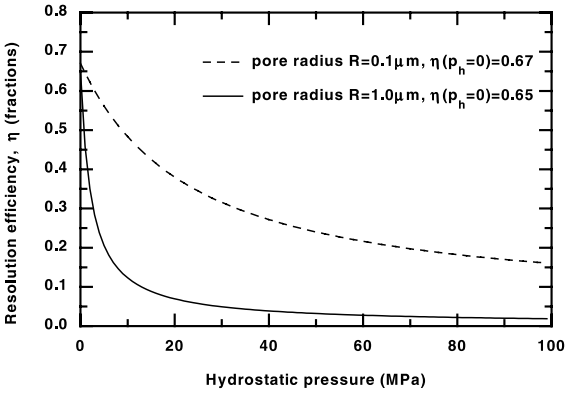


Fig. 1. The effect of the hydrostatic pressure on the resolution efficiency (Eq. (15)).

$$n_g^0=\frac{4\pi R_p^3}{3}\frac{p_s}{k_BT_s}, \tag{16}$$

where $p_s$ and $T_s$ are, respectively, the sintering pressure and temperature. Because of its great mobility the hydrogen accumulated inside the pores can migrate easily and it cannot sustain the pressure induced by the pore surface.

The fission gas accumulated during the irradiation is insoluble in the matrix. Consequently, the pores do not disappear so time they are not so small that can be sputtered by interaction with the fission spikes.

Because of the fuel densification, the pore size distribution function becomes time dependent $f(r^3)\to f(r^3,t)$ and from the continuity condition,

$$\frac{\partial f}{\partial t}+\frac{\partial}{\partial r^3}\left(f\frac{dr^3}{dt}\right)=0. \tag{17}$$

But the pore volume will decrease in time as a result of the vacancies migration to the outer surfaces. So, it is not possible to give a satisfactory solution of the fuel densification using Eq. (17). Rather than the using a pore size distribution function, Assmann and Stehle [2] have proposed to evaluate the time evolution of the radius of the average volume pores from every class of a pore size frequency histogram, which is representative for a fuel manufacturer. Based on their proposal we developed a method that use instead of the time-evolution of average volume pores from every size class from the histogram [2], the time evolution of the boundaries radius $(R_{p,k-1},R_{p,k})$ of every class of pore sizes. Then the contribution to the porosity changes can be easily quantified using the formula [47]

$$P(t)=P_0-\frac{\pi}{3}\sum_{k=1}^{M}N_V^k(R_{p,k}+R_{p,k-1})(R_{p,k}^2+R_{p,k-1}^2);$$
$$N=\sum_{k=1}^{M}N_k. \tag{18}$$

Using Eq. (18) to evaluate the remaining porosity eliminates the requirements of building of intermediary pore size frequency histograms to establish the new average volume radius as a result of the different kinetics of pore size changes, as previously recommended by Assmann and Stehle [1,2]. When the smallest radius of a class interval from the histogram goes to zero then the new class frequency must be calculated using the following expression:

$$N_k'=N_k\frac{R_{p,k}'}{R_{p,k}-R_{p,k-1}}. \tag{19}$$

Eq. (19) has been established according to the uniform character of the distribution inside every frequency class. Both the values $N_k'$, the new class frequency and $R_{p,k}'$, the new largest radius of the size class (the radius on

the left of the interval is zero), correspond to the new time step interval.

## 4. Thermal re-sintering and gaseous swelling of the initial porosity

Two particular situations when both the fission rate $F$ and the resolution parameter $b$ can be taken zero, the thermal re-sintering tests on as-fabricated fuel pellets and respectively the out-of-pile annealing tests on irradiated fuel will be discussed below.

Let first study the form of Eq. (12) applied to the simpler case of thermal re-sintering in hydrogen atmosphere. In this case the gas pressure inside the pores can be neglected, the fission term in Eq. (12) disappear and the parameters $a^2$ and $b$ become

$$\begin{aligned} a^2 &= 4\pi C_B \overline{R}_p + z_v \rho_d, \\ b &= C_v^{eq}\left\{a^2 + 8\pi\gamma\Omega C_B/k_B T\right\}. \end{aligned} \tag{20}$$

Substituting Eq. (20) in Eq. (10) and the later one in Eq. (12), after the arrangement of terms we will have

$$\begin{aligned} &\frac{dR_p^3}{dt} = 3\alpha\left(\frac{R_p}{R_c} - 1\right); \quad R_c = \overline{R_p} + B; \quad \alpha = \frac{2\gamma\Omega D_v^{th} C_v^{eq}}{k_B T}; \\ &B = \frac{1/A + z_v\rho_d}{4\pi C_B}. \end{aligned} \tag{21}$$

From Ref. [16] the dislocation density in pure crystals is very low, for semiconductors it is $>10^6/m^2$, and it increases in worked polycrystalline metals to $\sim 10^{13}/m^2$. During the re-sintering process we will accept that the dislocation density is lower than the term $1/A$ and we will neglect it for the moment. Its effect will be discussed later, in connection with the out-of-pile annealing tests.

By symmetry with the Lifshitz and Slyozov theory, the term $R_c$ has the significance of a critical radius. However, versus their theory, where the critical radius is equal any time with the average pore radius, we have to take into account a new term, noted $B$, which depends on material parameters resulted from Eq. (21). The weight of the parameter $A$, defined by Eq. (10) whose value calculated using the definitions from Ref. [29] is

$$A = A_1 \bar{r}_g^2; \quad A_1 \cong 845 \left(\bar{r}_g = \text{meters}\right), \tag{22}$$

where $\bar{r}_g$, the average radius of the fuel grains, can be evaluated as a function of the initial grain radius.

Apparently, the pore size distribution function would be the same as that derived from the model of Lifshitz and Slyozov [18]. But in such cases the fuel volume does not properly change. The identity $R_c = \overline{R}_p$ is a result of a constant volume fraction of particles in system. Consequently, the vacancies will migrate from the smaller pores to the greater ones with the void volume conservation. Lifshitz and Slyozov emphasized that their distribution function becomes valuable in the last stage of the sintering process only deeply inside the fuel matrix. Actually, an increased number of vacancies migrate to the grain boundaries with the global effect of pore shrinkage. Thus for an initial 10 μm grain size the term $1/A \sim 4.7 \times 10^{11}/m^2$. On the other hand the $B$ parameter is inverse proportionally with the pore concentration that in the case of the lot no. 288 was $C_B^{initial} \approx 2.2 \times 10^{16}/m^3$ (initial) and it goes down during the re-sintering process. The resulted $B$ parameter is $B \sim 21$ μm and, consequently, the critical radius $R_c \sim 22$ μm that will increase as a result of the pore concentration decreasing. That means that the all pores with radius smaller than the critical radius will decrease their size and only a very isolated pore size class of sizes >44 μm could increase in diameter. Because pores with radius greater than the resulted critical radius (22 μm) are not usual in high density oxide fuels, we can accept according to Eq. (21) and discussion above that the pores can only shrink and the effect of the average pore radius from the distribution on the critical radius is insignificantly. If the grains grow, the critical radius decreases with the physical significance that the vacancies migrate rather to other pores from the grain than to the grain boundary. In such cases, if the pores do not all disappear, their size distribution function will tend to that resulted from the Lifshitz and Slyozov theory [18]. Larger pores concentrations are not unusual in high-density oxide fuel if the average pore size from the distribution is smaller than in the case of the Romanian fuel pellets. Thus, at lower mean pore radius and the same value of the initial porosity the pores concentration could increase with many orders of magnitude. A pore population with the pore concentration $C_B \sim 10^{18}/m^3$ give in effect a value of the parameter $B \sim 0.2$ μm. Obviously, the average pore radius of a such population must be lower than 1 μm, but there are enough pores in the distributions greater than $R_c = \overline{R} + B$ and consequently they will increase according with Eq. (21). Hence, in the limits of an initial great pore population, very high grain size, and for very short times from the beginning of the re-sintering process Eq. (21) becomes similar with the Lifshitz and Slyozov model respectively $R_c = \overline{R}_p$.

Careful analyses of the effect of grain growth for grains with initial radius between (5–10 μm) as usual in oxide fuels show that it is however small and becomes important only for that pore size distributions with very large concentration of large size pores. In this case the grain growth will delay the pore shrinkage.

As a result of the irradiation a large population of dislocations will be induced in the fuel matrix and even if a great part of them will be annealed at the higher temperatures invoked by the out-of-pile annealing tests their density remain great enough and the $A$ parameter in Eq. (21) can be neglected. The reader can verify that

for a small argument $p\Omega/k_BT$ the exponential term in Eq. (9) can be approximated as $e^x \cong 1+x$ and substituting the parameters from Eq. (9) in Eq. (10), the latter becomes

$$C_v = C_v^{eq}\left\{\frac{1+4\pi\overline{R}C_B}{1/A+a^2}\left(\frac{2\gamma}{\overline{R}_p}-\frac{\overline{p_gR_p}}{\overline{R}_p}\right)\frac{\Omega}{k_BT}\right\};$$
$$a^2 = 4\pi C_B\overline{R}_p + z_v\rho_d; \quad \overline{p_gR_p} = \int_0^\infty R_p p_g(R_p) n(R_p)\,dR_p. \tag{23}$$

Because of the previous irradiation of the fuel the term $z_v\rho_d \sim 10^{13}/m^2$ and consequently $1/A \ll a^2$ in Eq. (23). It will result that Eq. (23) is the same with the White's expression of the average vacancies concentration from Ref. [43]. However, the term $1/A$ cannot be neglected when long-term annealing tests on samples with smaller bubbles concentration are simulated, because the second term in such situation tends to infinity. Besides, the physical significance of the problem disappears because we cannot measure volume changes into an infinite system as resulted from the White's treatment. In our treatment, the fuel is regarded as a fuel grains assembly in which the pore volume changes as a result of vacancies balance between bubbles, dislocations and grain boundaries, simultaneous with the grain growth in result of the mass transfer between the grains.

## 5. Application

The pore size frequency histograms will be used to evaluate the volume changes during the fuel pellets thermal re-sintering, gaseous swelling and densification.

Lets first study the as-described thermal re-sintering tests. To this aim we will write down Eq. (21) in the form

$$\frac{dR_p}{dt} = \frac{\alpha}{R_p^2}\left(\frac{R_p}{R_c}-1\right). \tag{24}$$

The solution of Eq. (24) is

$$\left(1+\frac{R_{p,0}}{R_c}\right)^2 - \left(1+\frac{R_p}{R_c}\right)^2 + 2\ln\left|\frac{(1+R_{p,0}/R_c)}{(1+R_p/R_c)}\right| = -\frac{2\alpha}{R_c^3}\Delta t, \tag{25}$$

where $R_{p,0}$, is the initial pore radius.

Eq. (25) has been applied to both the pore size distribution specific to the Romanian fuel (Fig. 2(a)) and the pore size distribution corresponding to the fuel pellets batch no. 288 (Fig. 2(b)). To verify the accuracy of the evaluations, the initial lognormal distributions have been divided in both equal length radius intervals and equal natural logarithm of radius intervals. The resulted histograms were used to evaluate the thermal parameters that give the best fit of the density measurements.

As expected, the using of size classes of equal length in radius involves a large number of classes for an accurate evaluation of the results versus the equal intervals in natural logarithm of radius. As for example, Fig. 3(a) and (b) illustrate the results obtained by applying Eq. (24) to initial frequency histogram characteristic of the Romanian fuel and respectively to the histogram characteristic to the 288 batch using both 50 classes of equal length in pore radius and 10 classes of equal intervals in natural logarithm of pore size. It can be seen in both Fig. 3(a) and (b) that a discontinuous line describing the fuel densification arises as a result of the discrete nature of the pore size distribution. The points where the densification

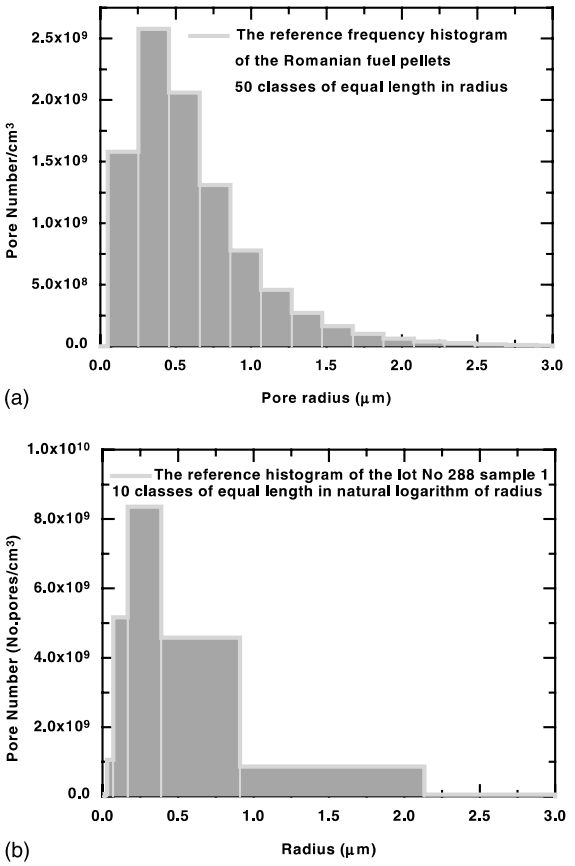


Fig. 2. (a) The pore size frequency histogram resulted by dividing the fitted lognormal distribution function of the Romanian fuel pellets fabrication route in classes of equal radius lengths. (b) The pore size histogram resulted by dividing the fitted lognormal distribution function of the fuel pellets lot no. 288 in classes of equal length of natural logarithm of radius.

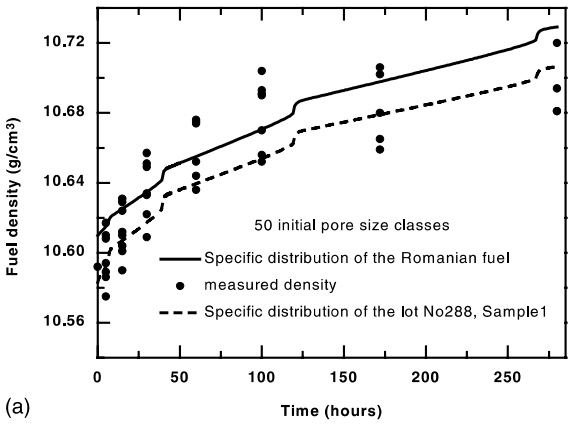


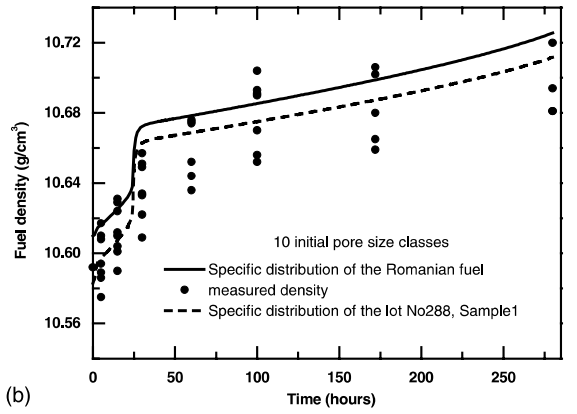


Fig. 3. (a) Time evolution of the $UO_2$ pellets, during the re-sintering tests measured and calculated using Eq. (23) and the pore size histograms similar with Fig. 2(a). (b) Time evolution of the $UO_2$ pellets, during the re-sintering tests measured and calculated using Eq. (23) and the pore size histograms similar with Fig. 2(b). The measured densities are given in Table 3.

is abruptly changed correspond to the disappearing of a size class of higher frequency from the histogram.

The diffusion parameters resulted by fitting the model (Eq. (24)) to our experimental results are the same as previously established by Reinfried [4]

$$D_{\mathrm{v}}^{\mathrm{th}} = 0.125\exp[-222\ (\mathrm{kJ})/RT];$$
$$D_{\mathrm{U}} = 5.0\times 10^{-3}\exp[-368\ (\mathrm{kJ})/RT]. \tag{26}$$

The experimental results used in Fig. 3(a) are from pellets density measurements by xylene immersion penetration method from fuel pellets batches no. 249, 271 and 288 (Table 3).

For a better description of the size class frequencies, a correction of the number of pores from every class has been made according to the formula [47]

$$N_{V,M-k} = N_{V,M-k} - \sum_{i=0}^{k} p_{M-k,M-i}N_{V,M-i};$$
$$p_{M-k,M-k+1} = \sqrt{1-\left(\frac{r_{M-k}}{r_{M-k+1}}\right)^2}, \tag{27}$$
$$p_{M-k,M} = \sqrt{1-\left(\frac{r_{M-k}}{r_M}\right)^2} - \sqrt{1-\left(\frac{r_{M-k+1}}{r_M}\right)^2},$$

where $P_{M-k,M-k+i}, i\in[0,M]$ is the probability of intersection of a pore with a plane situated between the pore size classes $M-k$, $M-k+i$ from its center, $r_i$ is the pore radius corresponding to the class $i$, on the frequency histogram.

The corresponding number from the unit volume has been calculated from the pore number measured in the class $i$ from the unit surface according to the formula [47]

$$\frac{N_{\mathrm{V}}^{\mathrm{K}}V_k}{\text{volume unity}} = \frac{N_{\mathrm{S}}^{\mathrm{K}}S_k}{\text{surface unity}} \Rightarrow N_{\mathrm{V}}^{\mathrm{K}} = N_{\mathrm{S}}^{\mathrm{K}}\frac{S_k}{V_k}$$
$$= N_{\mathrm{S}}^{\mathrm{K}}\frac{\left(R_{\mathrm{p},k}^2 + R_{\mathrm{p},k}R_{\mathrm{p},k-1} + R_{\mathrm{p},k-1}^2\right)}{\left(R_{\mathrm{p},k}+R_{\mathrm{p},k-1}\right)\left(R_{\mathrm{p},k}^2+R_{\mathrm{p},k-1}^2\right)}$$
$$= N_S^K\frac{\left(R_{\mathrm{p},k}^3 - R_{\mathrm{p},k-1}^3\right)}{\left(R_{\mathrm{p},k}^4 - R_{\mathrm{p},k-1}^4\right)}. \tag{28}$$

In Fig. 4 are shown the pore size frequency histograms corresponding to the fuel pellets from the lot no. 288 annealed at 1700 °C both measured and calculated using Eq. (24) after 15, 30 h and respectively 280 h thermal treatment. There are some discrepancies between the predicted and measured values but they must be attributed to the different form of the resulted size classes from calculation and the evaluation errors during the pore numbering. The densities predicted were however very closed versus the densities resulted from the xylene immersion method with only an exception after 280 h, where the density resulted after pore size corrections using Eq. (27) was greater than the measured one.

## 6. Fuel densification and swelling because of the initial porosity

It must be mentioned that in the Reinfried's model, to which the present paper has some similarities, neither the effect of vacancies migration by dislocations, nor the effect the pore radius and the hydrostatic pressure on the resolution parameter, nor the grain size distribution function whose main effect on the critical radius of pores shrinkage has been emphasized above, are accounted for. However the thermal diffusion

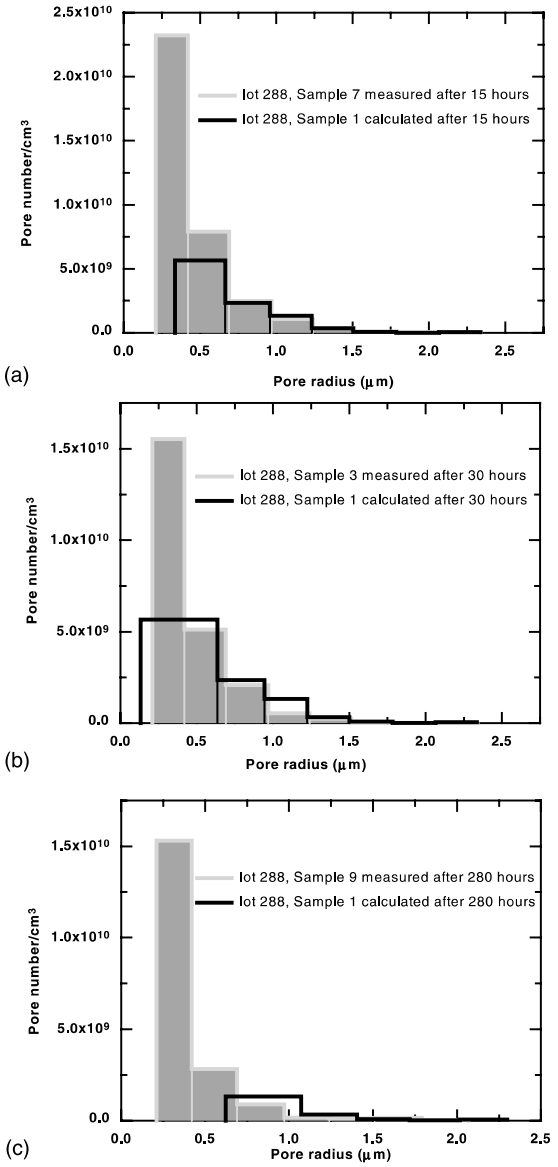


Fig. 4. Pore size frequency histograms corresponding to the fuel pellets from the lot no. 288 annealed at 1700 °C calculated and measured after (a) 15 h; (b) 30 h; (c) 280 h.

parameters that he used are the best values in our model of thermal re-sintering and we kept them for simulating the fuel densification and fuel swelling processes.

The temperature dependence of the dislocations density resulted from Ref. [3] is

$$\rho_d = 10^4 \exp[-2.07 \times 10^3 (T - 273) + 21.82] \ \left(1/m^2\right). \tag{29}$$

The number of vacancies per unit length of dislocation is $z_v = 24$ [16].

Before dealing with the general solution of the fuel densification resulted from the above evaluations (Eqs. (12)–(15)) let us study another particular situation, respectively the case of pores evolution during the post-irradiation annealing tests. The difference versus the thermal re-sintering is that the fission gas dissolved in the matrix will migrate to the pores according to the expression (13) in which the resolution parameter $b_0$ becomes zero. Also, the terms including the fission rate are taken zero.

Even using these simplifications, for simultaneous solving of the coupled Eqs. (12)–(15) a numerical scheme is only possible. Apart from numerical methods we can observe that for small fluctuations of pore radius and because the fission gas migration to the pores is governed by a slow process such the diffusion is, we can simplify the solution of Eq. (13) so that, by neglecting the fission gas pressure change inside the pore for a small change of the pore radius, it results in

$$\frac{dR_p}{dt} = -\frac{D_v^{th} C_v^0 \Omega}{k_B T}\left(\frac{A_2 R_p + A_3}{R_p^2}\right);$$
$$A_2 = \left(1 - \frac{C_v}{C_v^0}\right) + p_h - p_g; \quad A_3 = 2\gamma \tag{30}$$

and by integration,

$$\left(1 + \frac{R_{p,0}}{R_c}\right)^2 - \left(1 + \frac{R_p}{R_c}\right)^2 + 2\ln\left|\frac{\left(1 + R_{p,0}/R_c\right)}{\left(1 + R_p/R_c\right)}\right| = -\frac{2\alpha}{R_c^3}\Delta t, \tag{31}$$

where $R_c = -A_3/A_2$ and the average vacancies concentration $C_v$ is defined by Eq. (23). For a gas pressure dependence of pore radius of the form $p_g \sim R_p^{-3}$ it can be verified that the relative radius change $\varepsilon_r < 10^{-4}$ involve a relative pressure change $\varepsilon_p < 3 \times 10^{-4}$ that is enough small so that Eq. (31) becomes a very accurate approximation of the analytical solution.

Eq. (31) is the exact solution of a pore developing with a saturation limit of the fission gas inside. To avoid any ambiguity we emphasize that we do not use anywhere in our formalism this assumption. A pore developing with a saturation limit of the gas inside is however particularly for alpha particles (helium) during the fuel irradiation and the fuel storage [48]. We do not proposed to study the helium effect, but Eq. (31) can be used in such analyses.

The using Eq. (31) simplifies the evaluation method, because the changing of the pore radius during a temperature history can be done by simple evaluation of the time $\Delta t$ inside the relative error chosen $\varepsilon_r = \Delta R_p / R_{p0}$. When the time resulted is greater than the current time

step the corresponding pore radius is evaluated by linear interpolation between the as-supposed relative radius and the initial radius using the expression

$$R_{\mathrm{p,new}} = R_{\mathrm{p,initial}} + \Delta R_{\mathrm{p}} \frac{\Delta t_{\mathrm{step}}}{t(\Delta R_{\mathrm{p}})}, \tag{32}$$

where $t(\Delta R_{\mathrm{p}})$ is the time evaluated using Eq. (31) for a relative radius change $\Delta R_{\mathrm{p}}/R_{\mathrm{p,initial}} = \varepsilon_{\mathrm{R}}$.

At the end of the time step new evaluations of the fission gas atoms arrived inside the pore and the new gas pressures are done. At the end of the radius evaluation for every size class the formulas (18) and (19) are used to evaluate the porosity changes and respectively, the new size frequencies for that pore classes whose left margins disappeared. Also, the new values of $\overline{R}_{\mathrm{p}}$ and $\overline{R_{\mathrm{p}}^2}$ used to calculate the average concentration of vacancies are evaluated. A similar formalism as described above can be given to evaluate the changes of an arbitrary pore radius during the fuel densification.

Our aim is to see if the initial pores could become good sinks of the fission gas during the temperature gradients. For a good comparison with the re-sintering tests we choose for calculation the pore size frequency histogram specific to the lot no. 288 divided in 18 size classes of equal length in natural logarithm of radius. A first step of analyses consisted in simulating of the fuel densification in the same conditions as used in the thermal re-sintering tests (280 h at 1700 °C), but at various hydrostatic pressures and a neutron flux of $10^{13}$ n/cm$^2$ s. The results shown in Fig. 5(a) suggest that the hydrostatic pressure all the time controls the fuel densification, but the total fission gas accumulated in pores was insignificantly. The various forms of the lines representing the fission gas fractions from pores in Fig. 5(b) result from the discontinuous form of the pore size distribution.

Stronger effects can be observed at higher temperatures as it is shown in Fig. 6 where the fuel temperature was 1800 °C in the same irradiation conditions as previous defined for 1700 °C. It can be seen from Fig. 6(a) that the fuel density tends to the theoretical density of the $UO_2$ pellets faster than at 1700 °C and the fission gas fraction from pores increases with hydrostatic pressure increasing up to a maximum of ~40% (Fig. 6(b)).

The pore size distribution changed during the irradiation at 1700 °C, to a very large population of small bubbles of the same radius $R_{\mathrm{pore}} = 0.1$ μm whose number change slowly with the hydrostatic pressure from $C_{\mathrm{B}} \sim 1.9 \times 10^{16}/\mathrm{m}^3$ at $p_{\mathrm{H}} = 0$ MPa to $C_{\mathrm{B}} \sim 2.2 \times 10^{16}$ m$^3$ at $p_{\mathrm{h}} = 30$ Mpa (Fig. 7(a)). Similar situation can be followed in Fig. 7(b) for 1800 °C fuel temperature, where the most frequent pores radius was $R_{\mathrm{pore}} = 0.3$ μm and their number $C_{\mathrm{B}} \sim 2.1 \times 10^{16}/\mathrm{m}^3$ at $p_{\mathrm{H}} = 0$ MPa increased to $C_{\mathrm{B}} \sim 2.2 \times 10^{16}/\mathrm{m}^3$ for a pore radius $R_{\mathrm{pore}} =$ 0.2 μm at $p_{\mathrm{H}} = 30$ MPa. A very small number of initial

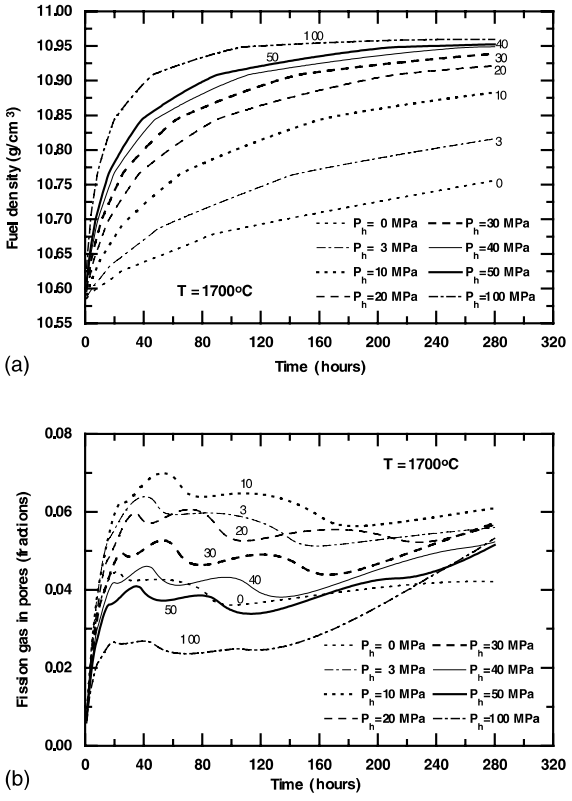


Fig. 5. Time evolution of the $UO_2$ fuel density (a), and of the fission gas accumulated in the remaining pores (b), at various hydrostatic pressures (280 h irradiation at 1700 °C and $10^{13}$ n/cm$^2$ s).

pores disappeared and it can be explained if we take into account that the initial average pore size was great enough (Fig. 7(a) and (b)). From the results presented above at the temperatures simulated, the initial pore concentration does not change too much.

Kashibe and Une performed annealing tests on high-pressure sintered pellets (50 and respectively 100 MPa) for one hour at 1500 °C $UO_2$ fuel temperature. Using our pore size distribution the model predictions in this case shown that the fuel density, the pore concentration and the pore mean radius did not change significantly, even if the hydrostatic pressure varied between 0–100 MPa. However, we cannot accurate evaluate their experiment because the pore size distribution is not completely defined in Ref. [8].

A base irradiation history of constant fuel temperature (1400 h at 1000 °C and 30 MPa hydrostatic pressure), followed by an out-of-pile test of the unconstrained fuel ($p_{\mathrm{h}} = 0$) consisting in 1 h ramp at 1650 °C and 30 h holding at this temperature has been simulated using the pore size distribution characteristic of the lot no. 288. It can be seen from Fig. 8 that the fuel density decreased

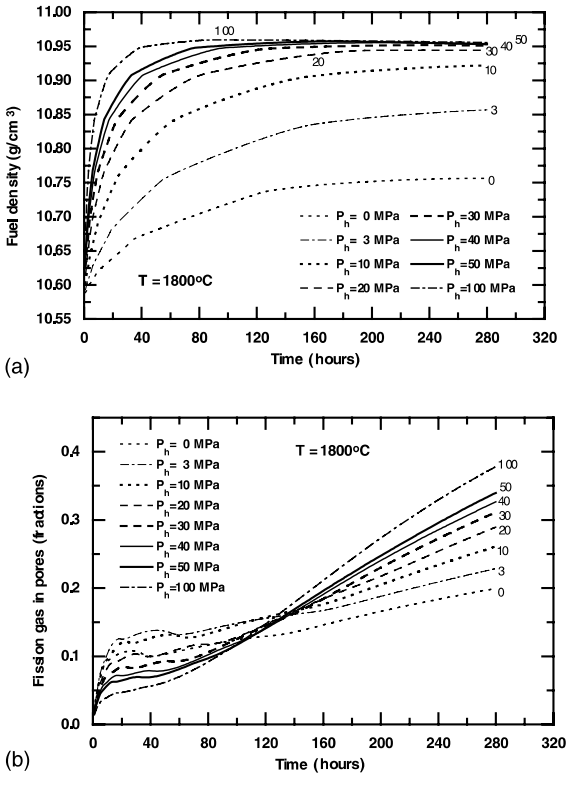


Fig. 6. Time evolution of the $UO_2$ fuel density (a), and of the fission gas accumulated in the remaining pores (b), at various hydrostatic pressures (280 h irradiation at 1800 °C and $10^{13}$ n/cm$^2$ s).

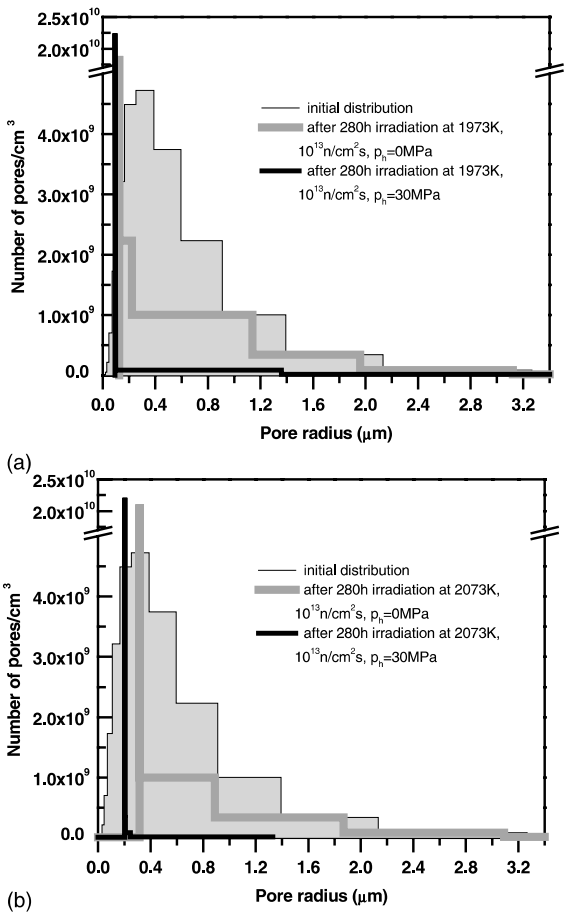


Fig. 7. Pore size distributions resulted after 280 h irradiation 1700 °C (a) and respectively 1800 °C (b) at hydrostatic pressures of 30 and 0 MPa and in neutron flux of $10^{13}$ n/cm$^2$ s.

from ~10.85 g/cm$^3$ at the end of irradiation to ~10.82 g/cm$^3$ at the end of the 30 h annealing at 1650 °C, while the amount of fission gas increase in pores from 0 to ~14%. The pore size distribution changed also drastically as it can be seen in Figs. 9 and 10 where the initial pore size distribution, the pore size distribution before the ramp test and after 30 h maintaining at 1650 °C are depicted. From our evaluation a large population of pores with sizes between 1.2 and 600 nm will remain in the fuel after 1400 h. Its smallest limit will shortly increase from ~1.2 nm (Fig. 9) to ~16 nm (Fig. 10), during the 0.2 °C/s temperature transient at 1650 °C (~1 h) without any changes of the other limit (600 nm). The initial pore concentration $C_B^{initial} \approx 2.2 \times 10^{16}$ /m$^3$ changed after the base irradiation to $C_B^{final} \approx 0.7 \times 10^{16}$ /m$^3$. The mentioned size pore class (~1.2 nm) represents about 50%. After 30 h annealing at 1650 °C, the smallest pores will increase significantly and arrive at ~0.7 μm.

Using a similar expression of the average vacancy concentration as given in Eq. (23), and the supposition that under extreme vacancy starvation of the matrix the intra-granular bubbles are all over-pressurized, White showed that during the annealing tests on irradiated fuel, the vacancies diffusivity will be reduced by a term proportionally with $z_v\rho_d/a^2$ [43] as a result of the vacancies starvation at the matrix/bubble interface. The same argument is done to explain the exponential tails of the distribution of the grown bubbles resulted from the tests described in Ref. [42] whose main consequence would be that a certain vacancy gradient is required to initiate absorption of vacancies and gas atoms in bubbles. He invokes a selective absorption probability where only a proportion of the intra-granular bubbles may absorb gas and vacancies. White arrives at an expression of the absorption probability of vacancies in bubbles from which a bubble size distribution function can be given [43].

Cornell and Turnbull shown very convincingly the manner in which a pore is destroyed by interaction with the fission fragments in their pictures noted Figs. 3 and 4 from Ref. [26], but the pictures also show a greater concentration of nanometer size bubbles around the

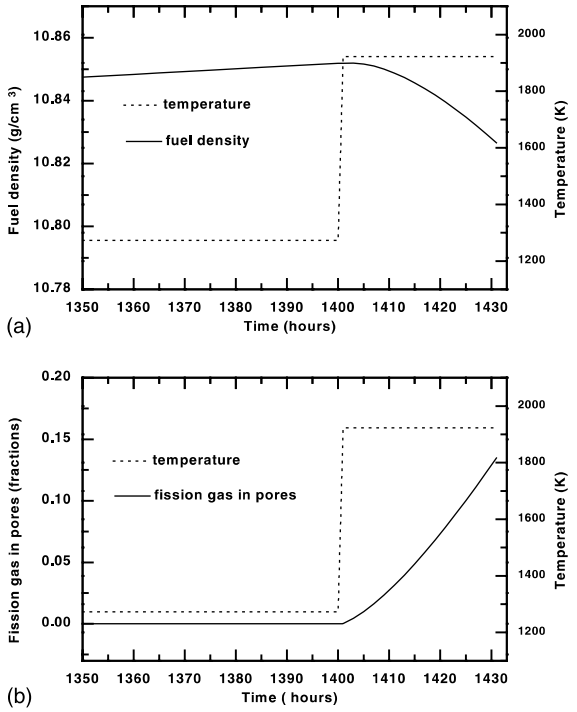


Fig. 8. Time evolution of the $UO_2$ fuel density (a), and of the fission gas accumulated in the remaining pores (b), at 30 MPa hydrostatic pressures after 1400 h base irradiation at 1000 °C and an out-of-pile test of the unconstrained fuel (one hour ramp at 1650 °C followed by 29 h holding at 1650 °C, $p_h = 0$).

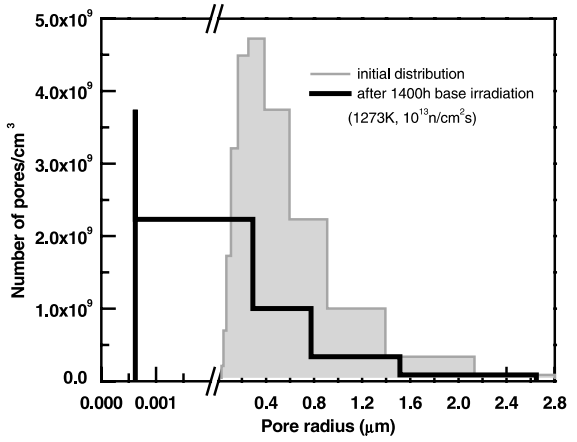


Fig. 9. The pore size distribution at the beginning and at the end of 1400 h base irradiation at 1000 °C and at 30 MPa hydrostatic pressures in a neutron flux of $10^{13}$ n/cm$^2$ s.

pore in discussion in those pictures than in the rest of the fuel pellet fragment. That means that the bubble concentration is not as homogeneous as it is considered in the most of the analyses dedicated to the intra-granular

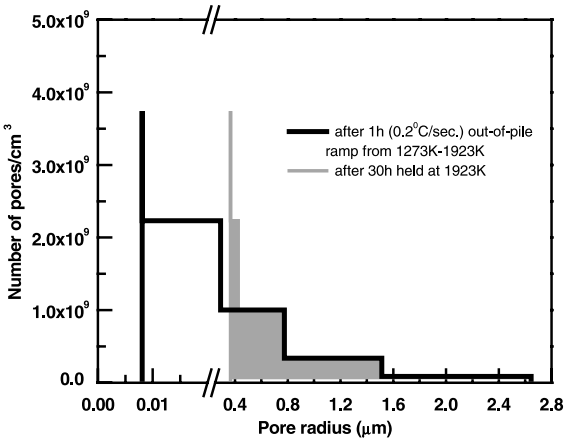


Fig. 10. The pore size distribution at the end of 1-h annealing test (0.2 °C/s) from 1000 °C and at the end of 30 h holding at 1650 °C.

bubbles behavior. So, without neglecting other sources and mechanisms that could initiate the larger bubble population, we think that a careful analysis of the regions in which as-fabricated pores existed is necessary because they had, and may still have, different bubbles and vacancies concentration long time after the pore disappearing. To verify this simple assumption, the pores that disappeared in our evaluation ($\sim 1.5 \times 10^{16}$ /m$^3$) up to the end of 1400 h base irradiation at 1000 °C, have been transformed into single intra-granular bubbles class at the observed 1 nm size and their time evolution was studied in the same formalism attributed to the densification-swelling mechanism of the initial porosity. So, we kept them in consideration at this size and followed their evolution along the irradiation time. According to the Harisson equation of state for Xe [22], the gas relative density in bubbles fluctuated up to the maximum 3.4. They did not increase on the all irradiation time, but during the annealing tests the bubble population grown to the same sizes as the pore size class with the smallest size limit respectively to $\sim$16 nm after an hour transient temperature at 1650 °C. Having in mind that the resulted concentration of the grown bubbles was up to five orders of magnitude lower than the usually $10^{23}$–$10^{24}$/m$^3$ nanometer bubbles, after the annealing tests described in Ref. [42], it is not absurd to suppose that a large part of the increased intra-granular bubbles raises from the initial as-fabricated porosity or from that regions where that pores existed previously.

## 7. Conclusions

An accurate analysis of the fuel density by both image analyses and immersion methods proved that the

sintered $UO_2$ pellets from the Romanian route of the CANDU type fuel fabrication can be well characterized by a specific lognormal form of the pore volume distribution function. The well-characterized $UO_2$ pellets used to evaluate the pore volume distribution function were annealed at 1700 °C and the time evolution of the fuel density and of the pore size distribution was measured for various time intervals between 5 to 280 h. The results proved that the pore volume distribution does not conserve its initial lognormal form. The alternative method of building the pore size frequency histograms, recommended for using in thermal, densification and gas swelling evaluations of the oxide fuel was careful analyzed. The most difficult problem in such time-dependent analyses rises from the necessity to build intermediary pore volume frequency histograms and to re-arrange the size classes because the class's size limits do not change in time with the same rate. To this aim a corrected porosity formula has been proposed based on the uniform character of the distributions in every size class from the histogram.

Supplementary analyses proved that the efficiency of the irradiation-induced resolution will decrease with about one order of magnitude because of the hydrostatic pressures generated by the mechanical contact fuel-cladding, and this effect cannot be neglected in evaluation of the fission gas migrated inside the pores during the fuel irradiation. A corrected formula has been proposed.

Theoretical evaluation of the existing methods of calculating the fuel densification proved that there is an inconsistent treatment of the average vacancy concentration. To arrive at a correct evaluation of the time dependence of the rate of the radius changing of an arbitrary pore, a new method has been proposed. Essentially, the method uses a complete homogenization of vacancies sources and sinks taking into account the polycrystalline nature of the oxide fuels. Thus, the average vacancy concentration becomes dependent on the initial grain size and grain growth, dislocation density, pore size distribution, etc.. The method simplification to thermal re-sintering process by neglecting the initial gas content of the pores and the irradiation terms proves the same form of the rate of the pore changes as in the Lifshitz and Slyozov model, but the pore volume distribution function cannot be the same. Moreover, it has been proved that the pores radius can only decrease during the thermal re-sintering process for lower initial pore concentration and correspondingly greater average pores radius. Particular situations could locally give an apparent pore size distribution of the same form with that previously described by the Lifshitz and Slyozov model but only deeply inside the large grains and for a larger initial pore concentration.

The method permits also one to study the weights of the grain size distribution function and the dislocation densities during both the thermal re-sintering tests and the fuel irradiation.

The predicted results versus the thermal re-sintering tests described in Ref. [8] shown very low-density fluctuations with the hydrostatic pressure but we used a very different pore size distribution.

When the grain size term is neglected, the similarity between the expression of the average vacancy concentration previously established by White is obvious and in the limit of a high dislocation density the two models have the same form when the intra-granular gas swelling is analyzed.

An annealing test on irradiated fuel has been simulated and the model predictions shown an increased number of bubbles of the same size even at the beginning of the temperature transient. The assumption that the former as-fabricated pores could create favorite regions in the matrix from which the intra-granular bubbles can grow has been also verified.

Of course, along with the densification-swelling model of the initial porosity from oxide fuels presented above, adequate models of inter-granular bubbles growth and interlinkage and models fission gas migration to the grain boundary are required to simulate the fuel behavior during irradiation.

## Acknowledgements

This paper has been carried out under a research contract between the International Atomic Energy Agency and the Institute for Nuclear Research, Pitesti, Romania.

## References

[1] H. Stehle, H. Assmann, J. Nucl. Mater. 61 (1976) 326.
[2] H. Assmann, H. Stehle, J. Nucl. Mater. 48 (1978) 49.
[3] C.C. Nichols, F.A. Dollins, J. Nucl. Mater. 78 (1978) 326.
[4] D. Reinfried, A simple microstructure dependent model for in-reactor densification of $UO_2$, ZIK 436, March 1981.
[5] G.J. Small, Densification of uranium oxide during thermal reactor irradiation, BNES Conference on Nuclear Fuel Performance, Stratford upon Avon 1985.
[6] G.J. Small, J. Nucl. Mater. 148 (1987) 302.
[7] Y. Bouguerra, A. Si-Ahmed, J. Nucl. Mater. 178 (1991) 300.
[8] S. Kashibe, K. Une, J. Nucl. Sci. Techn. 35 (11) (1998) 796.
[9] I.J. Hastings, T.J. Caster, R. Dosieva et al., AECL, MISC, 250, 1983.
[10] I.J. Hastings, AECL, MISC, 249, 1982.
[11] N. Hopp, M. Billaux, J. Van Vilet, COMETHE III-L General Description, BN-89201.
[12] M.C. Paraschiv, Romanian irradiation tests, OECD/IAEA, IFPE DataBase, 2001.
[13] St. Mehedinteanu et al., Internal Report INR, RI-2309, 1986.

[14] C. Gheorghiu et al., Internal Report INR, RI1274, 1983.
[15] A. Paraschiv, M. Paraschiv, S. Ion, Internal Report INR RI-2764, 1989.
[16] D.R. Olander, Fundamental Aspects of Nuclear Reactor Fuel Elements, ERDA, USA, 1976.
[17] I. Popov, C. Gentea, L. Stoica, C. Hadanceanu, Internal Report INR RI-2744, 1989.
[18] I.M. Lifshitz, V.V. Slyozov, J. Phys. Chem. Solids 19 (1/2) (1961) 35.
[19] M.V. Speight, Philos. Mag. 32 (1975) 1101.
[20] H.R. Warner, F.A. Nichols, Nucl. App. Techn. 9 (1970) 148.
[21] R.J. White, M.O. Tucker, J. Nucl. Mater. 118 (1983) 1.
[22] J.W. Harisson, J. Nucl. Mater. 31 (1969) 99.
[23] R.M. Cornell, Philos. Mag. 19 (1969) 539.
[24] A.D. Wapham, Philos. Mag. 23 (1971) 987.
[25] J.A. Turnbull, J. Nucl. Mater. 38 (1971) 203.
[26] R.M. Cornell, J.A. Turnbull, J. Nucl. Mater. 41 (1971) 87.
[27] J.A. Turnbull, R.M. Cornell, J. Nucl. Mater. 41 (1971) 156.
[28] M.V. Speight, Nucl. Sci. Eng. 37 (1969) 180.
[29] M.C. Paraschiv, A. Paraschiv, F. Glodeanu, J. Nucl. Mater. 246 (1997) 223.
[30] H. Blank, J. Nucl. Mater. 58 (1975) 123.
[31] M.H. Wood, M.R. Hayns, AERE R.8153, February 1976.
[32] M.J.F. Notley, I.J. Hastings, AECL, 5838, 1978.
[33] R. Bullough, D.R. Haries, M.R. Hayns, J. Nucl. Mater. 88 (1980) 49.
[34] M.H. Wood, J.R. Matthews, TP-825, AERE Harwell, January 1980.
[35] M.H. Wood, J.R. Matthews, A.M. Jones, J. Nucl. Mater. 107 (1982) 327.
[36] D.A. MacInnes, I.R. Brearley, J. Nucl. Mater. 107 (1982) 123.
[37] P.T. Elton, P.E. Coleman, D.A. MacInnes, J. Nucl. Mater. 135 (1985) 63.
[38] C. Ronchi, J. Nucl. Mater. 148 (1987) 316.
[39] K. Une, J. Nucl. Mater. 158 (1988) 123.
[40] D. Hull, D.E. Rimmer, Philos. Mag. 4 (1959) 673.
[41] C.T. Walker, P. Knappik, M. Mogensen, J. Nucl. Mater. 160 (1988) 123.
[42] C. Baker, R. Corcoran, A.T. Donaldson, R.J. White, EHPG meeting Loen, May 1996.
[43] R.J. White, The growth of intra-granular bubbles in post-irradiation annealed $UO_2$ fuel', IAEA Meeting, Windermere, UK, June 2000.
[44] J.H. Evans, Modelling of fission gas bubble migration to grain boundaries during post irradiation annealing in high burnup $UO_2$, IAEA Meeting, Cadarache, France, September 2001.
[45] R.W. Grimes, C.R.A. Catlow, Phil. Trans. R. Soc. Lond. A 335 (1991) 609.
[46] R.L. Coble, J. Appl. Phys. 32 (1961) 787.
[47] M.C. Paraschiv, Philosophy thesis.
[48] J.P. Piron, M. Peletier, J. Pavageau, Helium behaviour in spent $UO_2$ and MOX fuels, IAEA Meeting, Cadarache, France, September 2001.
[49] R. Weston, J.M. Wright, S.B. Fisher, G.A. Gates, Progress on SBR MOX fuel development, Topfuel 2001, Stockholm, Sweden.